# Study of the excitation energy partition based on the prompt neutron multiplicity*

Dong-Ying Huo (霍东英)[1] Kang Wu (吴康)[1] Zheng Wei (韦峥)[1,2,3†] Jun-Run Wang (王俊润)[1,2,3]
Yu Zhang (张宇)[1,2,3] Ze-En Yao (姚泽恩)[1,2,3] Xiang-Zhou Cai (蔡翔舟)[4] Jin-Gen Chen (陈金根)[4]
Xun-Chao Zhang (张勋超)[5] Han-Jie Cai (蔡汉杰)[5]

[1]School of Nuclear Science and Technology, Lanzhou University, Lanzhou 730000, China
[2]Engineering Research Center for Neutron Application Technology, Ministry of Education, Lanzhou University, Lanzhou 730000, China
[3]MOE Frontiers Science Center for Rare Isotopes, Lanzhou University, Lanzhou 730000, China
[4]Shanghai Institute of Applied Physics, Chinese Academy of Sciences, Shanghai 201800, China
[5]Institute of Modern Physics, Chinese Academy of Sciences, Lanzhou 730000, China

**Abstract:** In this study, the scission point model is employed to characterize the configuration of the dinuclear system at the scission point, thereby enabling determination of the intrinsic excitation energy at which the system separates during fission. Following the full acceleration of the fragments and the relaxation of their shapes to equilibrium, a sustained neutron evaporation process was calculated using the statistical evaporation model. This allowed for the derivation of the average neutron multiplicity as a function of fission fragment mass, including its dependence on the initial excitation energy of the compound nucleus. The extent of agreement between theoretical predictions and experimental measurements provides insight into the excitation energy partition among the fragments at the scission point.

**Keywords:** neutron-induced fission, excitation energy partition, prompt neutron multiplicity, scission point model

**DOI:** 10.1088/1674-1137/ae7dc0 **CSTR:** 32044.14.ChinesePhysicsC.50094106

## I. INTRODUCTION

Although 80 years have elapsed since its discovery [1–2], nuclear fission continues to be a subject of significant interest in theoretical research [3−5]. In particular, actinides are important nuclear fuels for fission devices. Data on their prompt fission observables, such as independent fission yields, multiplicities, and energy spectra of prompt neutrons and $\gamma$ rays, are the key inputs for determining burnup and transmutation system [6]. In recent years, research on prompt fission observables has advanced significantly, including the development of the Monte Carlo codes FIFRELIN [7] and CGMF [8] based on the Hauser-Feshbach model, as well as the phenomenological GEF model [9] and the Los Alamos model [10].

The total energy released during low-energy nuclear fission is predominantly manifested as the kinetic energy of the fission fragments. A more critical aspect lies in the transient deformation energy and intrinsic excitation energy within these fragments. These energy components not only determine the nuclear state of the fragments at the moment of scission but also profoundly influence subsequent processes of neutron evaporation, gamma decay, and the overall evolutionary trajectory of the fission products.

The degree of excitation of the fission fragments has long been puzzling because it appears to differ from simple statistical expectations. Prompt neutrons are emitted on an extremely short timescale and carry away most of the fissioning system's excitation energy. Consequently, the prompt neutron multiplicity serves as a direct indicator of the fragment excitation energy. Given that the probability of neutron emission is highly sensitive to nuclear temperature, even small differences in excitation energy can lead to substantial variations in neutron multiplicity [11−12]. As a result, the dependence of prompt neutron yield on the fragment mass number emerges as a key observable for probing the mechanisms underlying fission energy partition.

The prompt neutron multiplicity is very sensitive to

Received 8 April 2026; Accepted 16 June 2026; Accepted manuscript online 17 June 2026

* Supported by the National Natural Science Foundation of China (12547141), the NSFC-Nuclear Technology Innovation Joint Fund (U2167203), the Fundamental Research Funds for the Central Universities (lzujbky-2025-jdzx11, lzujbky-2023-stlt01), the National Key Laboratory of Neutron Science and Technology (NST202401016), and the Major Science and Technology Projects of Gansu Province (22ZD6GB020)

† E-mail: weizheng@lzu.edu.cn

the characteristics of the primary fragment configurations. Fortunately, in the last decade, substantial progress has been made in the scission point model [13−20] of nuclear fission, which can now calculate and reproduce primary fragment distributions. In our previous studies, we improved the scission point model [21−23] by considering the octupole deformations of the fission fragments. This advancement enables more accurate calculations of fragment yields and descriptions of fragment deformation in neutron-induced fission of typical actinides.

In this paper, we aim to integrate the statistical evaporation model with the scission point model to describe the prompt neutron multiplicity. The paper is organized as follows. In Sec. II, we first describe the scission point model and the statistical evaporation model adopted in this study. The calculated prompt neutron observables, together with a discussion of the results, are given in Sec. III. A summary of this study is presented in Sec. IV.

## II. METHOD

We assume that all prompt neutrons are evaporated from fully accelerated, excited fission fragments. The evaporation is treated within the Weisskopf formula, considering each fragment as a thermalized liquid drop [10, 24−25]. After neutron absorption and subsequent fission of the compound nucleus, the primary fragments de-excite through successive neutron evaporation processes until their excitation energies are exhausted. The maximum energy $\varepsilon_{\rm m}$ available to an evaporated neutron equals the initial excitation energy of the emitting fragment $E^*$. Consequently, the neutron spectrum extends from zero to this kinematic limit. Let $n(\varepsilon)$ denote the energy spectrum of the outgoing neutrons as a function of energy $\varepsilon$. Then the number of outgoing neutrons in the energy range of $\varepsilon \to \varepsilon + {\rm d}\varepsilon$ is ${\rm d}N(\varepsilon) \to n(\varepsilon){\rm d}\varepsilon$.

The neutron spectrum is jointly governed by three independent factors: the probability that the fission fragment decays into a specific neutron-emission channel $\Gamma$, the level density $\rho(\varepsilon)$, and the residual excitation energy $\varepsilon \to \varepsilon + {\rm d}\varepsilon$ for this level density. Consequently,

$$n(\varepsilon){\rm d}\varepsilon \propto \Gamma\rho(\varepsilon){\rm d}\varepsilon. \quad (1)$$

Within the Hauser–Feshbach statistical formalism [26]

$$\Gamma \propto \varepsilon\sigma(\varepsilon), \quad (2)$$

where $\sigma(\varepsilon)$ denotes the cross section for compound-nucleus formation. In this study, this is replaced by the capture cross section extracted from the inverse (neutron-emission) reaction. The level density is parameterized by the conventional Fermi-gas expression $\rho(\varepsilon) \propto {\rm e}^{\sqrt{\varepsilon a}}$, where $a$ is the level-density parameter. Consequently,

$$n(\varepsilon){\rm d}\varepsilon \propto \varepsilon\sigma(\varepsilon){\rm e}^{-\varepsilon/T}{\rm d}\varepsilon, \quad (3)$$

where $T = \sqrt{\dfrac{\varepsilon}{a}}$ represents the nuclear temperature and $a$ is the level-density parameter in the Fermi-gas model. The prompt-neutron spectrum is

$$n(\varepsilon) \propto \varepsilon\sigma(\varepsilon){\rm e}^{-\varepsilon/T}. \quad (4)$$

After normalization, the neutron energy spectrum in the center-of-mass (CM) frame according to the Weisskopf–Ewing evaporation model [27] is

$$\phi(\varepsilon) = k(T)\varepsilon\sigma(\varepsilon)\exp(-\varepsilon/T), \quad (5)$$

with the temperature-dependent normalization constant

$$k(T) = \left[\int_0^\infty \sigma(\varepsilon)\varepsilon\exp(-\varepsilon/T)d\varepsilon\right]^{-1}. \quad (6)$$

Therefore, the average energy of an evaporated neutron is

$$\langle\varepsilon\rangle = \int_0^\infty \varepsilon\phi(\varepsilon){\rm d}\varepsilon. \quad (7)$$

In this paper, the sequential neutron emission is assumed to continue until the excitation energy of the fragment falls below its neutron separation energy $S_n$ [28]. The $\gamma$ ray emission at lower excitation energies is not taken into account in the present work. The prompt neutron multiplicity $\nu$ refers to the mean total number of prompt neutrons evaporated from a fully accelerated fission fragment. Each neutron carries away, on average, the sum of the neutron separation energy $S_n$ and its kinetic energy $\langle\varepsilon\rangle$. Hence,

$$\nu = \frac{E^*}{S_n + \langle\varepsilon\rangle}, \quad (8)$$

where $E^*$ denotes the excitation energy of the fission fragment.

The intrinsic excitation energy distribution of the fission fragments is calculated using the scission point model [20−22], and the mean excitation energy is obtained by averaging over the deformation of the fission fragments

$$\langle E^*(A_i)\rangle = \frac{\int E^*(A_i,\beta_{2i},\beta_{3i})w(A_i,\beta_{2i},\beta_{3i}){\rm d}\beta_{2L}{\rm d}\beta_{2H}{\rm d}\beta_{3L}{\rm d}\beta_{3H}}{\int w(A_i,\beta_{2i},\beta_{3i})d\beta_{2L}d\beta_{2H}{\rm d}\beta_{3L}{\rm d}\beta_{3H}}, \quad (9)$$

where the intrinsic excitation energy at the scission point is the initial excitation $E^*_{CN}(E^*_{CN}=E_n+Q)$ minus the potential energy $U$

$$E^*(A_i,\beta_{2i},\beta_{3i})=E^*_{CN}-U(A_i,\beta_{2i},\beta_{3i}). \tag{10}$$

The deformation parameters are $\beta_{\lambda i}$, where ($\lambda$ = 2, 3; $i=L, H$) denote quadrupole and octupole deformations of the light and heavy fragments. The relative formation probability $w(A_i,\beta_{2i},\beta_{3i})$ for fragments with certain charge numbers, mass numbers and deformations can be described as [21−23]

$$w(A_i,\beta_{2i},\beta_{3i})=\exp[-\frac{U(A_i,\beta_{2i},\beta_{3i})}{T}]. \tag{11}$$

Because the fragments are still excited at the scission point, their total excitation energy also incorporates the deformation energy $E_i^{def}$ released when the nascent fragments relax from the scission-point configuration to their respective ground-state shapes

$$E^{def}(A_i,\beta_{2i},\beta_{3i})=B(A_i,\beta_{2i},\beta_{3i})-B(A_i,\beta_{gs}), \tag{12}$$

where $B(A_i)$ represents the binding energy of the fission fragments [20−22]. The mean value is also calculated by averaging over the fragment deformations

$$\langle E^{def}(A_i)\rangle = \frac{\int E^{def}(A_i,\beta_{2i},\beta_{3i})w(A_i,\beta_{2i},\beta_{3i})\mathrm{d}\beta_{2L}\mathrm{d}\beta_{2H}\mathrm{d}\beta_{3L}\mathrm{d}\beta_{3H}}{\int w(A_i,\beta_{2i},\beta_{3i})\mathrm{d}\beta_{2L}\mathrm{d}\beta_{2H}\mathrm{d}\beta_{3L}\mathrm{d}\beta_{3H}}. \tag{13}$$

After scission, the fragments are accelerated by their Coulomb repulsion, and their shapes relax towards the ground-state shapes. It is assumed that the relaxation of the shapes occurs on a shorter timescale than the subsequent neutron evaporation. Once the fragments have separated, the deformation potential energy associated with the stretched configuration is rapidly released as the fragments relax to their ground states. This irreversible process almost completely converts the energy originally frozen in the shape degree of freedom into the intrinsic excitation energy of each fragment. Since the fracture cuts off the nuclear force connection, this part of the energy cannot be converted back into collective motion or redistributed among the fragments. It can only be released internally through particle evaporation, thereby becoming an additional and non-shareable energy source for prompt neutrons [29]. The intrinsic excitation energy is shared between the light and heavy fragments $E_i^{'*}$, and the prompt neutron multiplicity is expressed as

$$\nu=\frac{E^{'*}+\langle E^{def}\rangle}{S_n+\langle\varepsilon\rangle}. \tag{14}$$

The mean energy of prompt neutrons is given by

$$\langle\varepsilon\rangle=\int_0^\infty \varepsilon\phi(\varepsilon)\mathrm{d}\varepsilon = \frac{2}{T_m^2}\int_0^\infty \varepsilon^2\sigma(\varepsilon)\mathrm{d}\varepsilon\int_0^{T_m} k(T)T\exp(-\varepsilon/T)\mathrm{d}T. \tag{15}$$

The normalization constant is calculated as

$$k(T)=\left[\int_0^\infty \sigma(\varepsilon)\varepsilon\exp(-\varepsilon/T)\mathrm{d}\varepsilon\right]^{-1}. \tag{16}$$

$T_m$ denotes the maximum nuclear temperature of the residual nucleus, which is related to its excitation energy

$$T_m=\sqrt{\frac{E^{'*}-S_n}{a}}. \tag{17}$$

The mechanism of intrinsic excitation energy sharing among the fragments is a heavily debated topic. To study the mechanism of excitation energy distribution from a macroscopic perspective, we neglect the initial excitation energy by setting the incident neutron energy to $E_n$=0. Let $R_T=T_L/T_H$ denote the ratio of the nuclear temperature of the light fragment to that of the heavy fragment. Under the assumption that thermal equilibrium is established among the intrinsic degrees of freedom of each fragment, the partition of the intrinsic excitation energy can be derived. The first assumption postulates that the two fragments have equal nuclear temperatures (Fermi-gas), $R_T=1$,

$$\frac{E^*}{a_{CN}}=\frac{E_L^{'*}}{a_L}=\frac{E_H^{'*}}{a_H}. \tag{18}$$

Under this condition, the intrinsic excitation energy is partitioned in proportion to their mass ratio, and the excitation energy of each fission fragment is given by $E_{L,H}^{'*}=\frac{a_{L,H}}{a_{CN}}E^*$.

The other assumption uses the non-isothermal model proposed by Ohsawa [30], in which $R_T$ scales linearly with fragment mass number and governs the partition between the two complementary fragments, as in Refs. [31−35]. The fragment excitation energy is then expressed as

$$E_L^{'*}=\frac{E^*}{1+\dfrac{a_H}{a_L R_T^2}}, \tag{19}$$

$$E_H'^* = \frac{E^*}{1+\dfrac{a_L R_T^2}{a_H}}, \tag{20}$$

where the ratio $R_T$ is theoretically motivated by the deformation of the fission fragments. This phenomenon was also explained by K-H Schmidt *et al*. [36]. The shell correction varies drastically with deformation. The more negative the shell correction, the more severely the level density is compressed; consequently, the total excitation energy is shifted to the companion fragments. For $n$+$^{235}$U, the doubly magic fragment ($^{132}$Sn) has a shell correction of –9.8 MeV, and almost all the intrinsic energy goes into the light fragment. Similarly, the $^{78}$Ni ($Z$=28, $N$=50 shell closure) fragment is close to the magic number. Therefore, the excitation energy is strongly biased toward the heavy fragment $^{158}$Gd. This distribution method forms a sharp contrast with the uniform splitting given by the Fermi gas model.

Accordingly, the maximum of $R_T$(A) occurs for heavy fragments with $A$≈132, where both deformation and temperature are minimal. Conversely, the minimum of $R_T$ occurs for light fragments near $A$≈78, which are again characterized by minimal deformation and temperature. Additionally, the ratio $R_T$ equals 1.0 for the fragments around the symmetric fission region. Figure 1 shows $R_T$(A) for the case of neutron-induced $^{235}$U fission at $E_n$=0. For the mass number dependence of $R_T$, we take $R_T$ around $A$ = 132 to be 1.6 and $R_T$ around $A$ = 154 to be 0.6.

## Ⅲ. RESULTS

In this section, the prompt neutron observables such as the mean energy of prompt neutrons $\langle\varepsilon\rangle$ and the prompt neutron multiplicity $\nu$ were calculated for neutron-induced fission of $^{235}$U, $^{237}$Np, and $^{239}$Pu using the scission point model coupled with the statistical evaporation model.

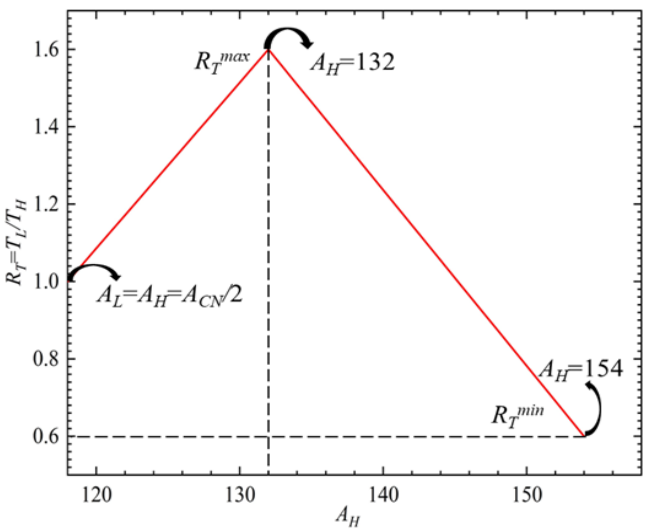


**Fig. 1.** (color online) $R_T\,(A)$ for neutron induced $^{235}$U fission at $E_n$=0.

Figures 2 and 3 compare the calculated average kinetic energies of prompt neutrons with experimental data [37−40]. The results are underestimated in the fission fragment mass range of $A_H$=125−135 with the level density parameter $a = A/11$. The average kinetic energy of a prompt neutron is related to the nuclear temperature. The shell effect of the fragments is significantly influenced by the nuclear temperature. We calculate the average kinetic energy of prompt neutrons using the Ignatyuk [40] level

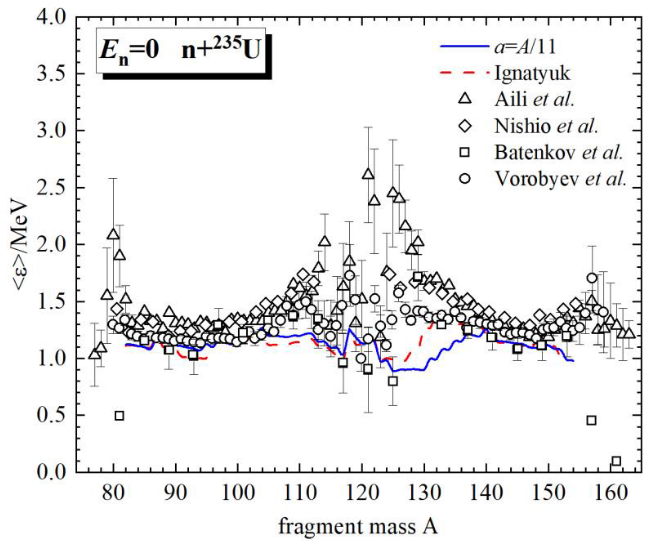


**Fig. 2.** (color online) Mean energy of prompt neutrons as a function of the fragment mass of $^{235}$U fission for different level density parameters.

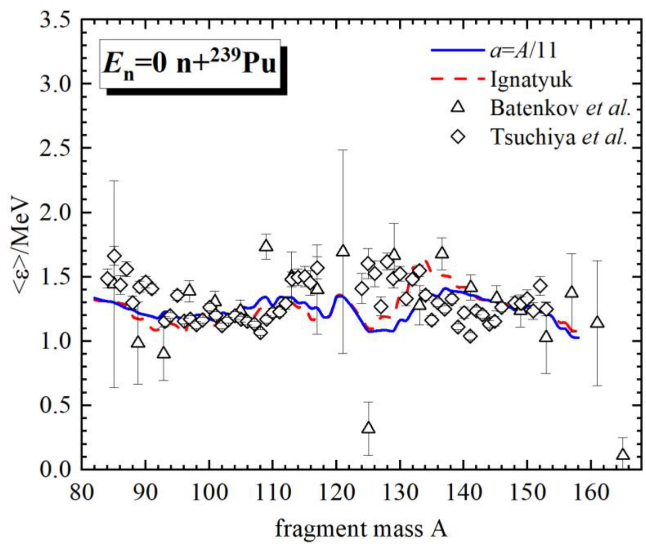


**Fig. 3.** (color online) Mean energy of prompt neutrons as a function of the fragment mass of $^{239}$Pu fission for different level density parameters.

density formula

$$a = \frac{A}{11}[1+\delta U^{\rm shell}/E^* * (1-\exp(-0.05E^*))], \quad (21)$$

which mainly accounts for the shell effect of the fission fragments. Figures 2 and 3 show the average kinetic energies of prompt neutrons obtained using different level density parameter models. Compared with the Fermi gas model, the Ignatyuk model results are significantly higher for fission fragment masses in the range of 125−135 and agree better with the experimental data.

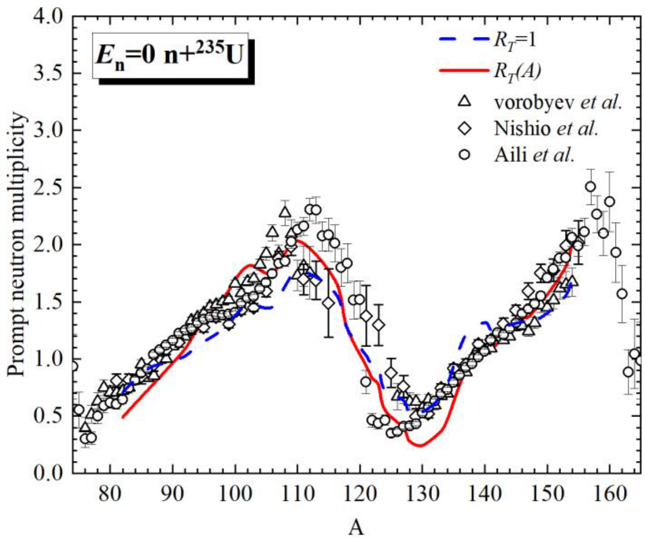


**Fig. 4.** (color online) Prompt neutron multiplicity as a function of the fragment mass of $^{235}$U fission, compared with the experimental data [38−41].

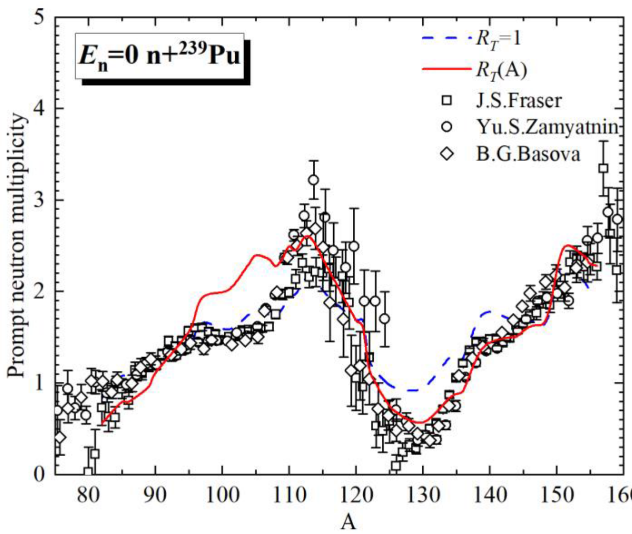


**Fig. 5.** (color online) Prompt neutron multiplicity as a function of the fragment mass of $^{239}$Pu fission, compared with the experimental data [42−43].

Figures 4 and 5 compare the calculated prompt neutron multiplicities for different excitation energy partitioning schemes with experimental data [38−41]. Under the assumptions of the two excitation energy allocation mechanisms, all theoretical calculations exhibit a pronounced saw-tooth structure. The total excitation energy of the fission fragments consists of two parts: the intrinsic excitation energy determined by the allocation model and the deformation energy related to the fragment's deformation state. Because magic nuclei have greater shell closure stability, their degree of deformation is significantly smaller than that of non-magic nuclei, resulting in a smaller contribution of deformation energy. Consequently, the total excitation energy reaches a local minimum, thereby minimizing number of neutrons emitted by the fragments in this mass region. This saw-tooth structure is a direct macroscopic signature of shell effects in the fission fragments.

As the incident neutron energy increases, calculations of prompt neutron multiplicities typically use the $E_n$=0 MeV results as a reference, and systematically analyse how the excess excitation energy is distributed between the fission fragments in order to determine the resulting neutron emission characteristics [44]. The major part of the energy released in low-energy fission is contained in the kinetic energy of the fission fragments. The rest is distributed between the deformation and intrinsic excitation energies of the nascent fragments. The additional incident-neutron energy is almost entirely converted into increased fragment excitation energy, while the total kinetic energy (TKE) remains essentially unchanged [44].

The enhanced neutron emission with increasing incident neutron energy is well known and has been observed for many fissioning systems [44−45]. The conventional approach assumes that the extra excitation is shared equally between the complementary fragments and uniformly scales the prompt neutron multiplicity distribution observed in $E_{\rm n}$=0 neutron induced fission to higher incident energies. However, the latest experimental measurements [46] and theoretical methods [29, 36, 44] consistently indicate that the excess neutrons originate mainly from heavy fragments, whereas the instantaneous neutron distribution of light fragments does not change with the incident neutron energy.

In this study, the hypotheses of two correction schemes are adopted to extract the prompt neutron multiplicity. The following denotations will be used to identify the neutron multiplicity distributions discussed below:

(i) Average method (AV). The increase in prompt neutron multiplicity as a function of incident neutron energy is equally distributed among all fission fragments.

(ii) Heavy method (HE). Starting from mass $A$=$A_{CN}$/2, the increase in prompt neutron multiplicity is distributed only among the heavy fragments, whereas the neutron multiplicity remains fixed for the light fission fragments as determined at $E_n$=0 MeV.

Figures 6−9 present the prompt neutron multiplicity distributions for neutron-induced fission of $^{235}$U and $^{237}$Np. The calculated curves exhibit optimal agreement with the experimental data [46] under the assumption of the HE method. With increasing incident neutron energy, the excess excitation energy shows a clear tendency to be preferentially channeled into the heavy fragments.

In this study, we assume that the two nascent fragments do not share the same temperature at the scission point. Instead, each fragment independently follows a constant temperature level density formula, resulting in distinct nuclear temperatures $T_L$ and $T_H$. Energy naturally flows from the higher-temperature fragment to the lower-temperature one, such that the intrinsic excitation energy ultimately accumulates entirely in the latter. Owing to its larger mass and higher level-density, the heavy fragment generally exhibits a lower temperature, $T_H$, compared to the light fragment, thereby acting as an "energy sink" that absorbs all the remaining excitation energy.

Calculations based on the two hypotheses proposed by A. Al-Adili *et al*. indicate that, as the incident neutron energy increases, fragments with lower nuclear temperat-

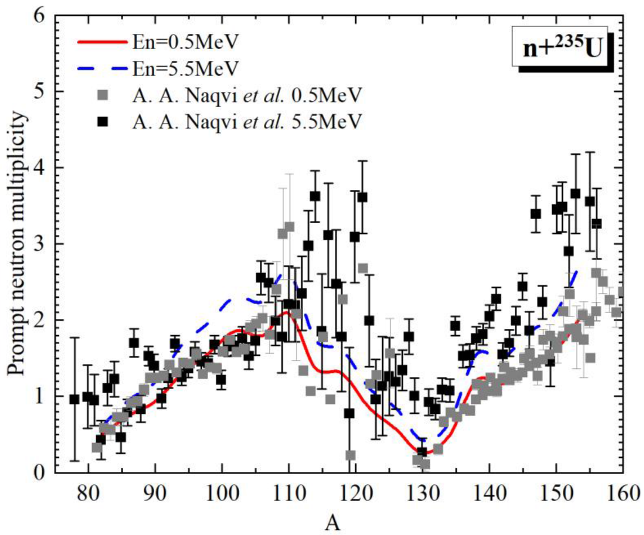


**Fig. 6.** (color online) Prompt neutron multiplicity distribution as a function of the fragment mass of $^{235}$U fission on AV method.

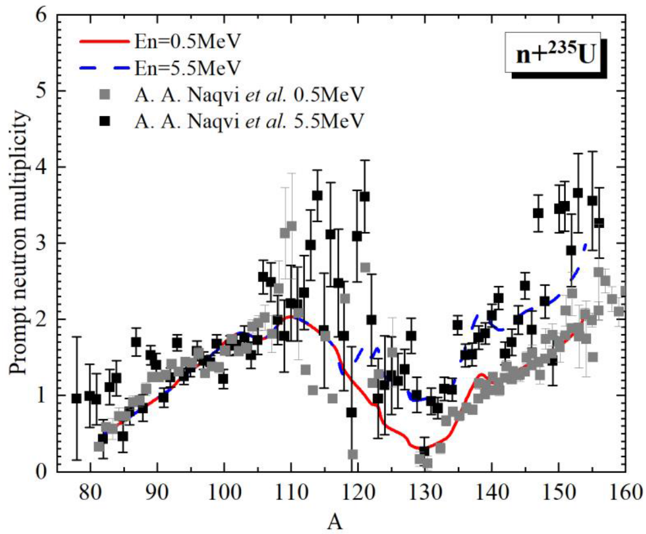


**Fig. 8.** (color online) Prompt neutron multiplicity distribution as a function of the fragment mass of $^{235}$U fission on HE method.

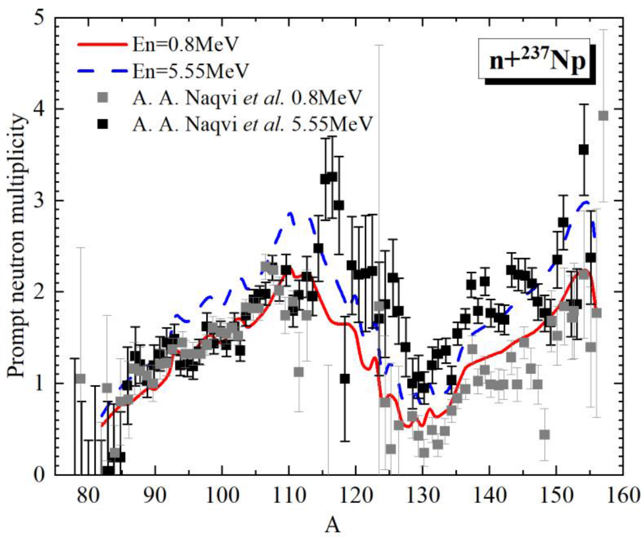


**Fig. 7.** (color online) Prompt neutron multiplicity distribution as a function of the fragment mass of $^{237}$Np fission on AV method.

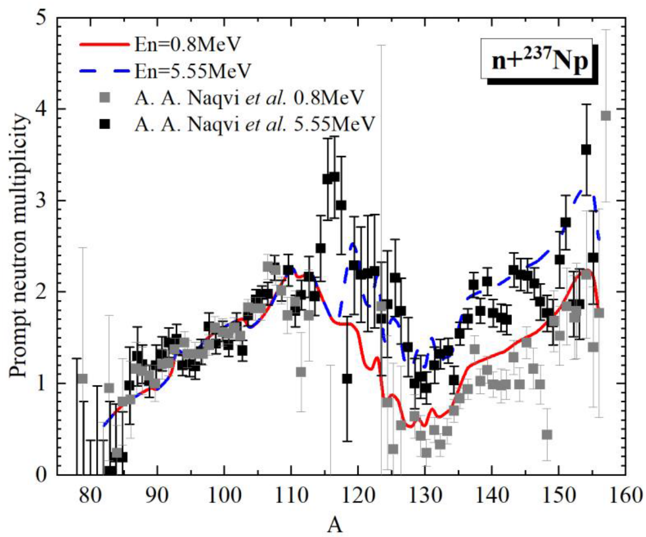


**Fig. 9.** (color online) Prompt neutron multiplicity distribution as a function of the fragment mass of $^{237}$Np fission on HE method.

ures can absorb more excitation energy. However, the nuclear temperature of every heavy fragment is not always lower than that of its light counterpart. Excitation energy is assumed to flow from the higher-temperature side to the lower-temperature side. The mechanism of energy partitioning considered here is the idealized "energy sorting mechanism" proposed in Ref. [36], in which all energy is transferred to one fragment, namely the one with the lowest temperature. Experimental data reveal that as the incident neutron energy increases to 5.5 and 5.55 MeV, the prompt neutron multiplicity distribution becomes increasingly non-uniform compared with the thermal-neutron case. The results in Figs. 10 and 11 accurately reproduce this trend, particularly the rise in the prompt-neutron multiplicity distribution for lighter fragments: in this region ($A_L$=80−85), the intrinsic nuclear temperature of the light fragment is lower than that of the heavy fragment; therefore, the entire excess flows into the light fragment, directly enhancing its neutron evaporation.

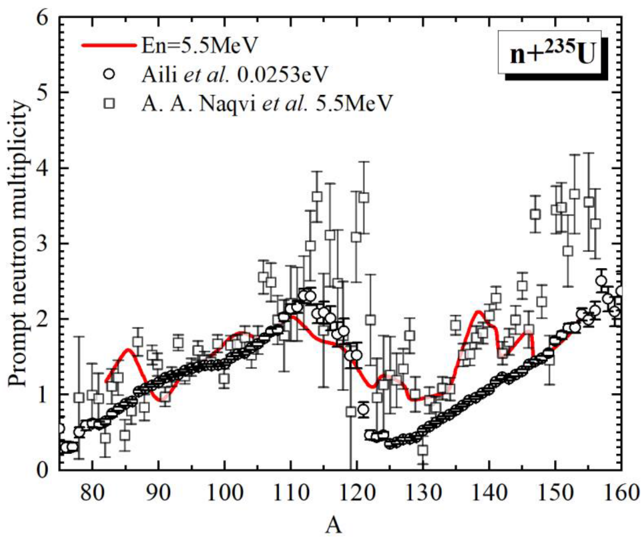


**Fig. 10.** (color online) Prompt neutron multiplicity distribution as a function of the fragment mass of $^{235}$U fission.

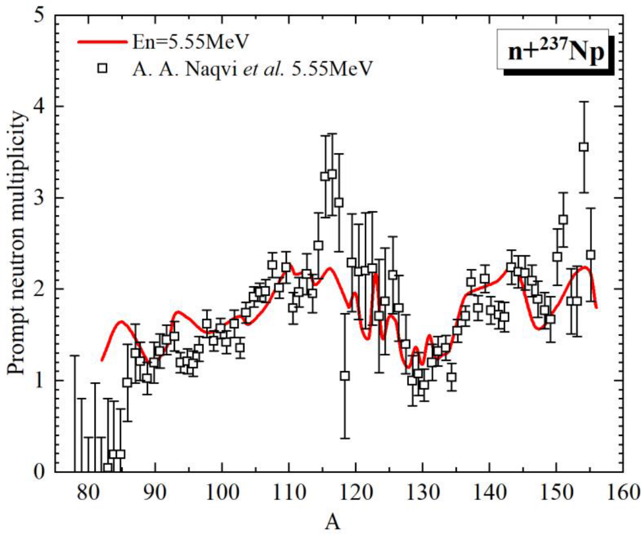


**Fig. 11.** (color online) Prompt neutron multiplicity distribution as a function of the fragment mass of $^{237}$Np fission.

These findings reveal that the partition of fission excitation energy between the light and heavy fragments does not conform to a simple constant-temperature model. Instead, it is sensitively governed by the instantaneous difference between their nuclear temperatures.

Notably, this study did not analyze the nuclear temperatures from a microscopic perspective. As the incident neutron energy was $E_n$=0 MeV, the ratio of the fragment nuclear temperature was assumed to take the value after energy partition. This value was then used to infer the direction of the excitation energy transfer at higher energies.

## IV. CONCLUSION

In this study, the scission point model is coupled with the statistical evaporation model in order to consistently describe the deexcitation process of primary fragments. The characteristics of the prompt neutron observables are well reproduced for neutron-induced $^{235}$U, $^{237}$Np, and $^{239}$Pu fission using the present model.

First, the mean energies of prompt neutrons and the prompt neutron multiplicity distributions for different excitation energy partition schemes were calculated for 0 MeV $n$+$^{235}$U and $^{239}$Pu fission. The calculations show reasonable agreement with the experimental data. The results demonstrate that the sawtooth pattern observed in the prompt neutron multiplicity distribution, particularly the periodic minima and maxima in neutron yield at certain mass numbers, arises from nuclear shell effects and fragment deformation energies rather than from statistical fluctuations. In regions corresponding to closed shells ($N$=82, $Z$=50), nuclei exhibit enhanced structural stability and reduced deformation, leading to less deformation energy being released during fission. This results in a local reduction in total excitation energy, which in turn manifests as a local minimum in the prompt neutron yield.

Furthermore, the results of the prompt neutron multiplicities for the two hypotheses by A. Al-Adili *et al*. are calculated for 0.8, 5.5 MeV $n$+$^{235}$U and 0.5, 5.55 MeV $n$+$^{237}$Np fission. As the incident neutron energy increases, the excess excitation energy shows a clear tendency to be preferentially channeled into the heavy fragment. Finally, the idealized "energy sorting mechanism" was considered, in which all energy is transferred to the fragment with the lowest temperature. The results agree with the experimental data. These findings demonstrate that the mechanism for the energy partitioning involves the transfer of energy to one fragment, namely the one with the lowest temperature. The energy sharing is therefore determined by the fragments' intrinsic level densities and their transient temperatures, rather than by a uniform statistical prescription.

In summary, the prompt neutron multiplicity serves not only as a direct indicator of the excitation energy stored in fission fragments but also as a critical observable for elucidating the mechanisms underlying energy partition in nuclear fission. Precise experimental measurements and theoretical modeling of the prompt neutron multiplicity distribution have significantly advanced the understanding of fission dynamics, thereby providing a robust physical basis for refining fission models, improving nuclear data evaluations, and enhancing neutron transport in reactor physics applications.

## References


[1] O. Hahn, F. Straßmann, Naturwissenschaften **27**, 11 (1939)
[2] L. Meitner, O. R. Frisch, Nature (London) **143**, 239 (1939)
[3] A. N. Andreyev, K. Nishio, and K. -H. Schmidt, Rep. Prog. Phys. **81**, 016301 (2018)
[4] K. -H. Schmidt, B. Jurado, Rep. Prog. Phys. **81**, 106301 (2018)
[5] N. Schunck, L. M. Robledo, Rep. Prog. Phys. **79**, 116301 (2016)
[6] L. Audouin, E. Pellereau, J. Taieb *et al.*, in *Nuclear Physics and GammaRay Sources for Nuclear Security and Nonproliferation* (Singapore: World Scientific, 2014), p. 217
[7] D. Regnier, O. Litaize, and O. Serot, EPJ Web of Conferences **42**, 04003 (2013)
[8] P. Talou, B. Becker, T. Kawano *et al.*, Phys. Rev. C **83**, 064612 (2011)
[9] D. G. Madland and J. R. Nix, Nucl. Sci. Eng. **81**, 213 (1982)
[10] K. -H. Schmidt, B. Jurado, C. Amouroux *et al.*, Nucl. Data Sheets **131**, 107 (2016)
[11] R. Vandenbosch and J. R. Huizenga, *Nuclear Fission* (San Diego: Academic Press, 1973)
[12] A. Al-Adili, F. -J. Hambsch, S. Pomp *et al.*, Phys. Rev. C **86**, 054601 (2012)
[13] B. D. Wilkins, E. P. Steinberg, and R. R. Chasman, Phys. Rev. C **14**, 1832 (1976)
[14] P. Fong, Phys. Rev. **135**, B1338 (1964)
[15] H. Pasca, A. V. Andreev, G. G. Adamian *et al.*, Phys. Rev. C **104**, 014604 (2021)
[16] H. Pasca, A. V. Andreev, G. G. Adamian *et al.*, Phys. Rev. C **101**, 064604 (2020)
[17] H. Pasca, A. V. Andreev, G. G. Adamian *et al.*, Phys. Rev. C **99**, 064611 (2019)
[18] H. Pasca, A. V. Andreev, G. G. Adamian *et al.*, Nucl. Phys. A **969**, 226 (2018)
[19] J. -F. Lemaître, S. Panebianco, J. L. Sida *et al.*, Phys. Rev. C **92**, 034617 (2015)
[20] J. -F. Lemaître, S. Goriely, S. Hilaire *et al.*, Phys. Rev. C **99**, 034612 (2019)
[21] D. Y. Huo, X. Yang, and C. Han, Chin. Phys. C **45**, 114104 (2021)
[22] D. Y. Huo, Z. Wei, K. Wu *et al*. Phys. Rev. C **108**, 024608 (2023)
[23] D. Y. Huo, Z. Wei, K. Wu *et al.*, Phys. Rev. C **109**, 064608 (2024)
[24] D. G. Madland, R. J. LaBauve, and J. R. Nix, Physics of neutron emission in fission, in *Proc. of a Consultants Meeting on Physics of Neutron Emission in Fission, Mito, Japan, 1988* (Vienna: IAEA, 1989), p. 259
[25] D. G. Madland, Post-scission fission theory, H4-SMR/1056-10, 11, Workshop on Nucl. Reac. Data and Nucl. Reactors, Physics, Design and Safety, ICTP-Trieste, Italy (1998)
[26] W. Hauser, H. Feshbach, Phys. Rev. **87**, 366 (1952)
[27] H. Delagrange *et al.*, Z. Phys. A **323**, 437 (1986)
[28] W. J. Huang, M. Wang, F. G. Kondev *et al.*, Chin. Phys. C **45**, 030002 (2021)
[29] K. -H. Schmidt, B. Jurado, Phys. Rev. C **83**, 061601(R) (2011)
[30] T. Ohsawa, T. Horiguchi, and M. Mitsuhashi, Nucl. Phys. A **665**, 3 (2000)
[31] O. Litaize, O. Serot, and L. Berge, Eur. Phys. J. A **51**, 177 (2015)
[32] S. Okumura, T. Kawano, P. Jaffke *et al.*, J. Nucl. Sci. Tech. **55**, 1009 (2018)
[33] A. E. Lovell, T. Kawano, S. Okumura *et al.*, Phys. Rev. C **103**, 014615 (2021)
[34] S. Tanaka, N. Nishimura, F. Minato *et al.*, Phys. Rev. C **108**, 054607 (2023)
[35] K. Fujio, A. Al-Adili, Eur. Phys. J. A **59**, 178 (2023)
[36] K. -H. Schmidt, B. Jurado, Phys. Rev. Lett. **104**, 212501 (2010)
[37] O. A. Batenkov, G. A. Boykov, F. -J. Hambsch *et al.*, AIP Conf. Proc. **769**, 1003 (2005)
[38] K. Nishio, Y. Nakagome, H. Yamamoto *et al.*, Nucl. Rhys. A, **632**, 540 (1998)
[39] A. Al-Adili, D. Tarrío, K. Jansson *et al.*, Phys. Rev. C **102**, 064610 (2020)
[40] A. Vorobyev *et al.*, EPJ Web Conf. **8**, 03004 (2010)
[41] A. V. Ignatyuk, G. N. Smirenkin, and A. S. Tishin, Sov. J. Nucl. Phys. **21**, 255 (1975)
[42] J. Fraser, J. Milton, Annu Rev Nucl Sci **16**(1), 379 (1966)
[43] Y. S. Zamyatnin, D. K. Rayaznov, B. G. Basova *et al.*, Yad. Fiz. 29, 595 (1979) (Soviet J. Nucl. Phys. 29, 305 (1979)
[44] M. Albertsson, B. G. Carlsson, T. Døssing *et al.*, Phys. Lett. B **803**, 135276 (2020)
[45] L. L. Liu, Y. J. Chen, N. C. Shu *et al.*, Phys. Rev. C **111**, 024607 (2025)
[46] R. Müller, A. A. Naqvi, F. Käppeler *et al.*, Phys. Rev. C **29**, 885 (1984)